ADVANCED FUNCTIONAL MATERIALS

Supporting Information

for *Adv. Funct. Mater.,* DOI: 10.1002/adfm.202112184

Sulfur-Treatment Passivates Bulk Defects in Sb_2Se_3 Photocathodes for Water Splitting

*Rajiv Ramanujam Prabhakar, Thomas Moehl, Dennis Friedrich, Marinus Kunst, Sudhanshu Shukla, Damilola Adeleye, Vinayaka H. Damle, Sebastian Siol, Wei Cui, Laxman Gouda, Jihye Suh, Yaakov R. Tischler, Roel van de Krol, and S. David Tilley**

SUPPORTING INFORMATION

Sulfur-treatment passivates bulk defects in Sb_2Se_3 photocathodes for water splitting

Rajiv Ramanujam Prabhakar,[1] Thomas Moehl,[1] Dennis Friedrich,[2] Marinus Kunst,[1] Sudhanshu Shukla,[3] Damilola Adeleye,[3] Vinayaka H. Damle,[4] Sebastian Siol,[5] Wei Cui,[1] Laxman Gouda,[1] Jihye Suh,[1] Yaakov R. Tischler[4], Roel van de Krol,[2] and S. David Tilley[1]*

[1] *Department of Chemistry, University of Zurich, Winterthurerstrasse 190, CH-8057 Zurich, Switzerland*

[2] *Institute for Solar Fuels, Helmholtz-Zentrum Berlin für Materialien und Energie GmbH, Hahn-Meitner-Platz 1, 14109 Berlin, Germany*

[3] *Laboratory for Photovoltaics, Department of Physics and Materials Science, University of Luxembourg, L-4422 Belvaux, Luxembourg*

[4] *Device Spectroscopy Laboratory, Department of Chemistry, Institute for Nanotechnology & Advanced Materials, Bar-Ilan University, Ramat Gan 5290000, Israel*

[5] *Empa Swiss Federal Laboratories for Materials Science and Technology, Überlandstrasse 129, CH-8600 Dübendorf, Switzerland*

*email: david.tilley@chem.uzh.ch

EXPERIMENTAL METHODS

Synthesis of Sb_2Se_3 thin films, sulfurization and material characterization: Sb metal was sputtered from a high purity Sb sputtering target to generate films of 300 nm thickness on quartz substrates for time resolved microwave conductivity (TRMC) measurements, and on Au-coated FTO substrates for dual working electrode measurements. Selenization and sulfurization procedures were the same as used in our previous work.[1] The crystal structure of Sb_2Se_3 and sulfur-treated Sb_2Se_3 was determined by X-ray diffraction using a Rigaku SmartLab instrument (Cu K_α radiation). UV–vis absorption spectra were measured using a PerkinElmer Lambda 950 spectrometer fitted with an integrating sphere. X-ray photoelectron spectroscopy (XPS) was conducted using a Physical Electronics (PHI) Quantum 2000 X-ray photoelectron spectrometer featuring monochromatic Al-Kα radiation, generated from an electron beam operated at 15 kV and 32.3 W. The energy scale of the instrument was calibrated using Au and Cu reference samples. The analysis was conducted at 1×10^{-6} Pa, with an electron take off angle of 45° and a pass energy of 46.00 eV. Charge compensation during the measurement was achieved using a low energy electron source. The sputter depth profile was performed using Ar ions (2 kV potential) on an area of approximately 4 mm^2. Surface elemental concentrations were determined using the instrument specific sensitivity factors for calculation. The core level emissions were fitted to deconvolute spectra with contributions from multiple elements using Voigt profiles (GL30) after Shirley background subtraction.

Time-resolved microwave conductivity measurements: TRMC measurements were performed by mounting the samples in a microwave cavity cell and placing within a setup similar to the one described.[2,3] A voltage controlled oscillator (SiversIMA VO3262X) generated the microwaves (X-band region, 8.4−8.7 GHz). During the measurements, a change in the microwave power ($\Delta P/P$) reflected by the cavity upon sample excitation by 3 ns (full-width at half-maximum) pulses of a wavelength tunable optical parametric oscillator (OPO) coupled to a diode-pumped Q-switched Nd:YAG laser at wavelengths between 350 and 1100 nm (50 Hz repetition rate) was monitored and correlated to the photoinduced change in the conductance of the sample, ΔG, given by

$$\frac{\Delta P(t)}{P} = -K\Delta G(t) \qquad (1)$$

where K is the sensitivity factor derived from the resonance characteristics of the cavity and the dielectric properties of the medium.

The change in photoconductance is related to the concentration of photogenerated charge-carrier pairs, eh_p, and the sum of their mobilities, $\sum\mu=\mu_e + \mu_h$, by

$$\Delta G = \beta e \sum\mu \int_0^L eh_p(z)\, dz, \qquad (2)$$

with β as a value determined by the cavity, L the thickness of the semiconductor, e as elementary charge and eh_p(z) as the concentration of photogenerated electron hole pairs at the depth z.

To relate the formation of photogenerated charge carriers to the photons absorbed, the quantum yield of charge carrier generation, ϕ_0, has to be defined:

$$\phi_0 = \int_0^L eh_p(z)\, dz / I_A \qquad (3)$$

with I_A being the photons absorbed per unit area. Latter is defined over optical measurements determining the fraction of converted photons:

$$F_A = I_A / I_0 = 1\text{-}R \qquad (4)$$

with R being the fraction of reflected incident light I_0.

Under the condition that the recombination, trapping and/ or immobilization of the charge carriers is slow compared to the actual pulse duration and characteristic reaction time of the cavity, the maximum photoconductance ($\Delta G_{max,0}$) reached after laser excitation can be defined as follows:

$$\Delta G_{max,0} = [\phi_0 \Sigma\mu] I_0 \beta e F_A \qquad (5)$$

And reformulated:

$$\phi_0 \Sigma\mu = \frac{\Delta G_{max,0}}{I_0 \beta e F_A} \qquad (6)$$

If, however, a decay (by recombination or trapping) of charge carriers already occurs on a time scale comparable to the response time of the cavity and during the laser pulse, the value $\phi\sum\mu$ is derived from the measurement of ΔG_{max} which will be a lower limit of the mobility:

$$\phi\Sigma\mu = \frac{\Delta G_{max}}{I_0 \beta e F_A} \leq \phi_0 \Sigma\mu \qquad (7)$$

The time dependent photoconductance is therefore defined (with normalization to the amount of generated electron hole pairs) as:

$$\frac{\Delta G}{I_0 \beta e F_A} \qquad (8)$$

Neutral density filters were selected to adjust the light intensity in the range of 10^9 – 10^{13} photons / pulse / cm^2.

Photoluminescence spectroscopy: Low temperature photoluminescence measurements were carried out in a home-built system equipped with a helium flow cryostat under 663-nm wavelength diode laser excitation source. The emitted luminescence was collected through off-axis positioned parabolic mirrors and focused into a fiber, and spectrally resolved by a monochromator and subsequently detected by a Si-charge-coupled device (CCD) and an InGaAs diode array. All the data were corrected with a calibration lamp with a known spectrum. Neutral density filters were used to vary the power for excitation intensity dependent PL.

Low frequency Raman spectroscopy (LFR): LFR measurements were carried out using an integrated laser and Volume Holographic (VHG) filter system (ONDAX, XLF-MICRO 532 nm) with 50 mW of optical power at an excitation wavelength of λ_{ex} = 532 nm. The laser output was routed into a lab microscope, and the Raman signal was fibre-coupled into an imaging spectrometer (Princeton Instruments, SP-2500i) with an EM-CCD camera (Princeton Instruments, ProEM 16002). Acquisition times of 5 seconds were used, and a grating groove density of 1800 g/mm was selected. The measurements were carried out by first setting the focus to the top surface and then slightly lowering the focal plane into the depth of the sample to avoid edge effects. At least 3 different regions were measured for each sample. The spectral baselines were shifted for presentation purposes. The integration time for spectral collection was 5 s per acquisition. Each spectrum was recorded by accumulating 3 frames, yielding an overall integration time of 15 s. The Raman frequencies were calibrated using a silicon wafer. All experiments were conducted at room temperature (293 K).

Dual-working electrode (DWE) fabrication: For DWE measurements, the Sb_2Se_3 was synthesized as described above. The main difference when compared to the conventional single working electrode setup is that a second working electrode (WE2, which measures the surface potential) is fabricated on the catalyst (Pt), which enables the determination of the photovoltage (the difference between the back contact potential (WE1) and the front contact potential (WE2)). The exposed Au-coated FTO served as the WE1 or back contact. To make the WE2 (or front contact), a 20 nm-thick Au layer was sputtered onto a part of the exposed Pt layer, as shown in

Figure S12. A copper wire was then connected to the Au via Ag paint as the WE2 and covered with another layer of epoxy for protection from the electrolyte.

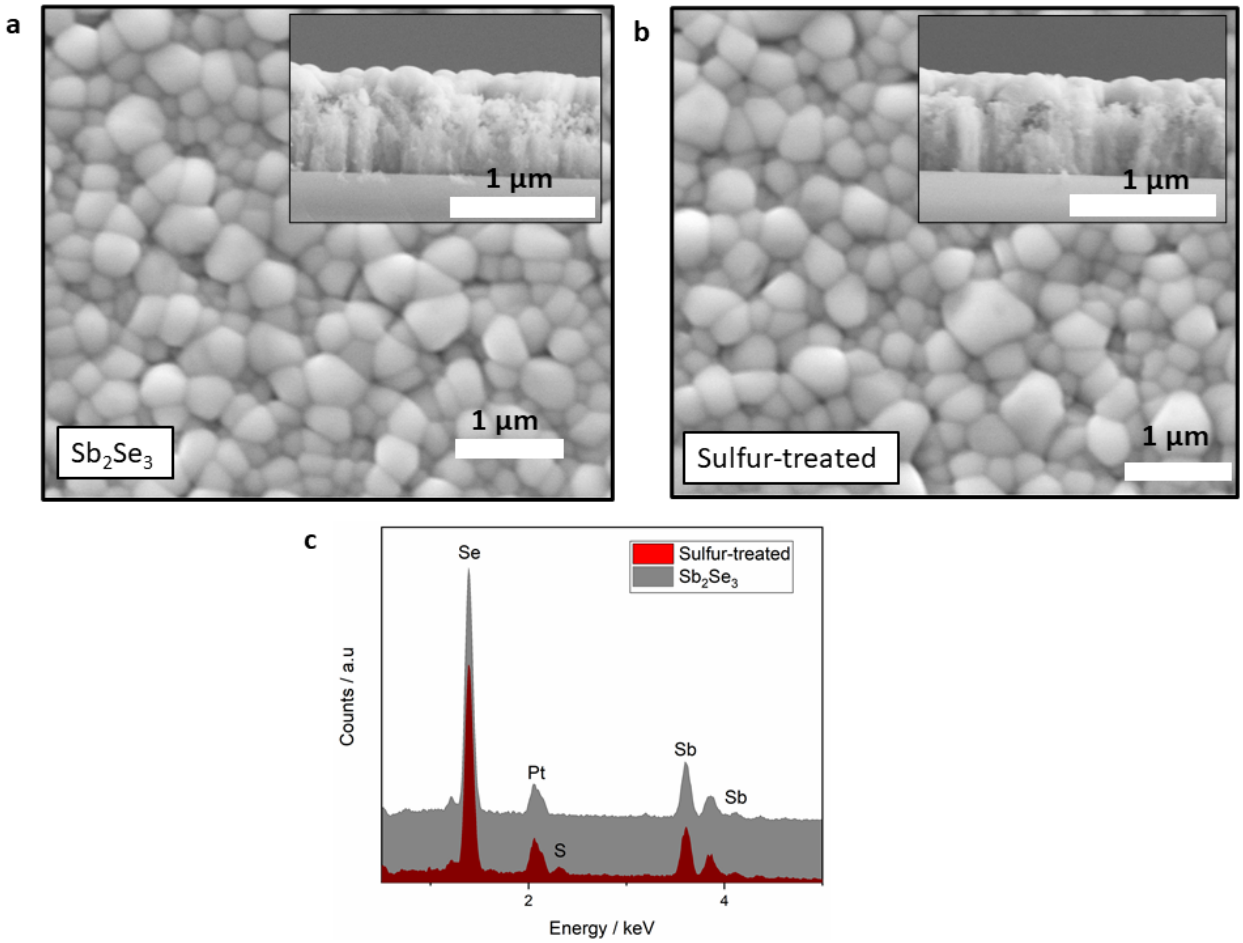

Figure S1. SEM plan view of **a** Sb_2Se_3, **b** sulfur-treated film (cross section of the films are provided in the inset). **c** EDX spectra of Sb_2Se_3 and sulfur-treated films. The EDX spectrum indicates the presence of sulfur in the sulfur-treated films as evidenced by the peak at around 2.3 keV (kα of sulfur). The Pt peak was due to Pt sputtered on the films for SEM imaging convenience (conductive coating as the quartz substrate is insulating).

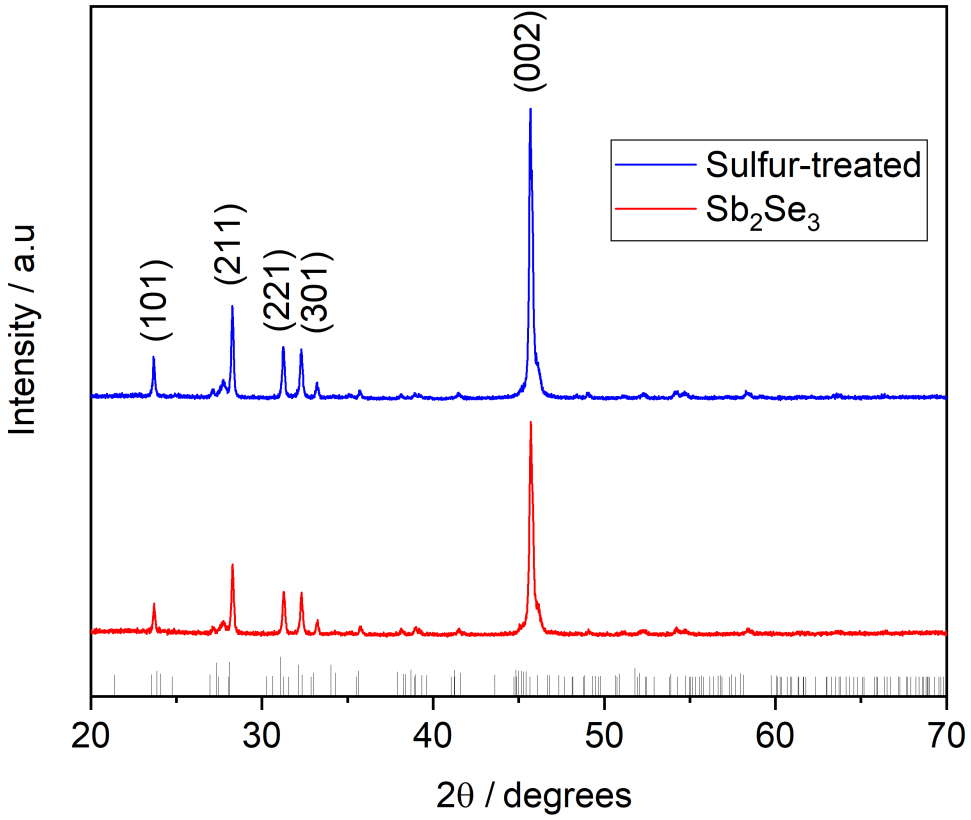

Figure S2. XRD pattern of Sb_2Se_3 and sulfur-treated films on quartz substrates. The crystallite size as obtained from the Scherrer equation was found to be 33.08 nm for the as-prepared Sb_2Se_3 film and 34.34 nm for the sulfur-treated sample.

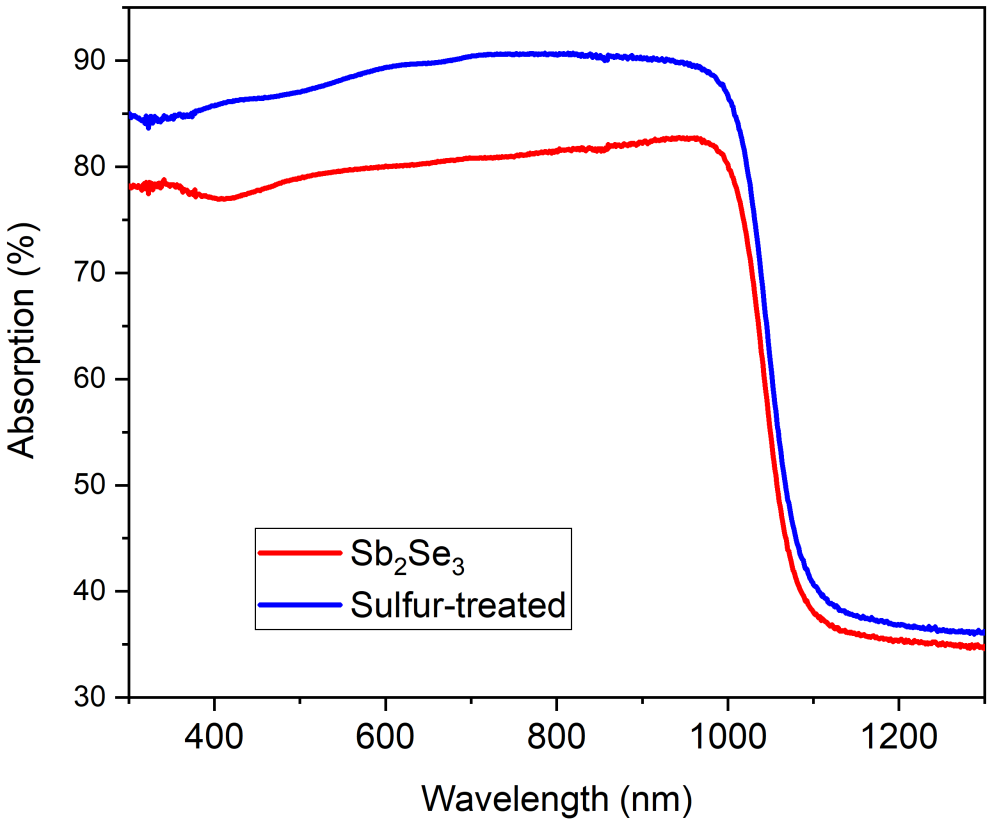

Figure S3. Absorption spectrum of Sb_2Se_3 and sulfur-treated films on quartz substrates (also used to estimate the fraction of absorbed photons in the TRMC experiments) shows a minor band gap shift of 0.01 eV for the sulfur-treated samples. The increased absorption in the sulfur treated sample is due to reduced reflectivity following sulfurization.

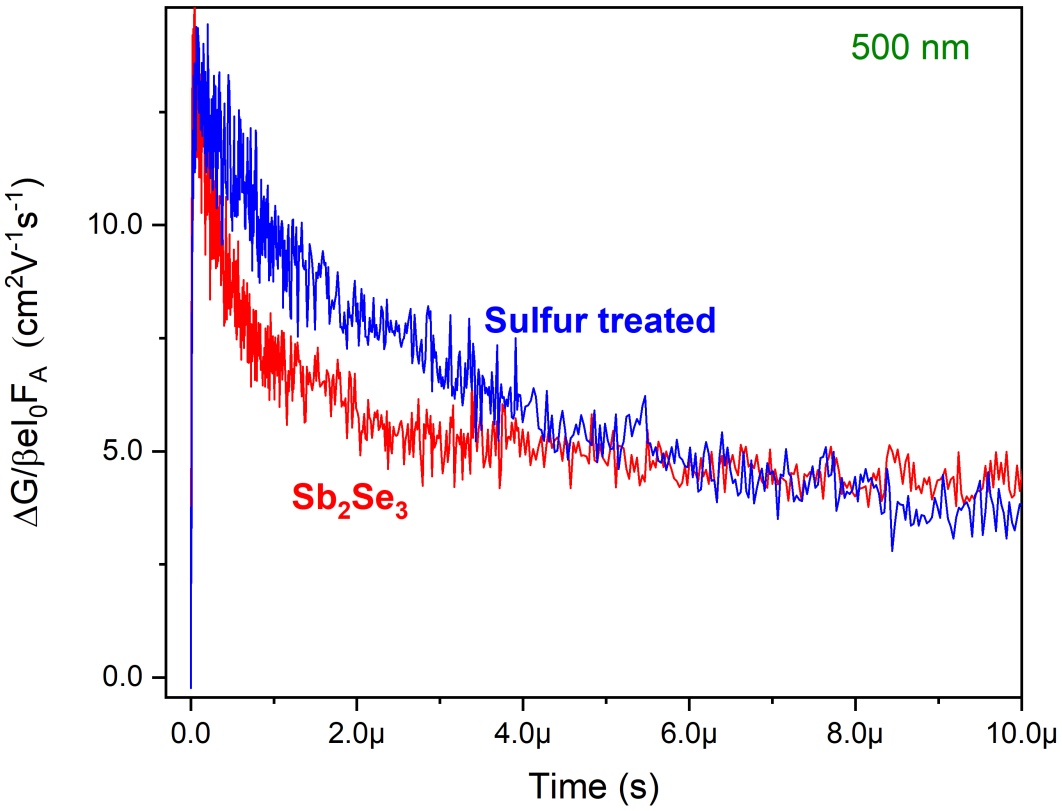

Figure S4. Photoconductance as a function of time for Sb_2Se_3 and sulfur-treated film at 500 nm (2.48 eV) excitation for a photon flux of 3.69 x 10^9 photons/cm^2 per pulse.

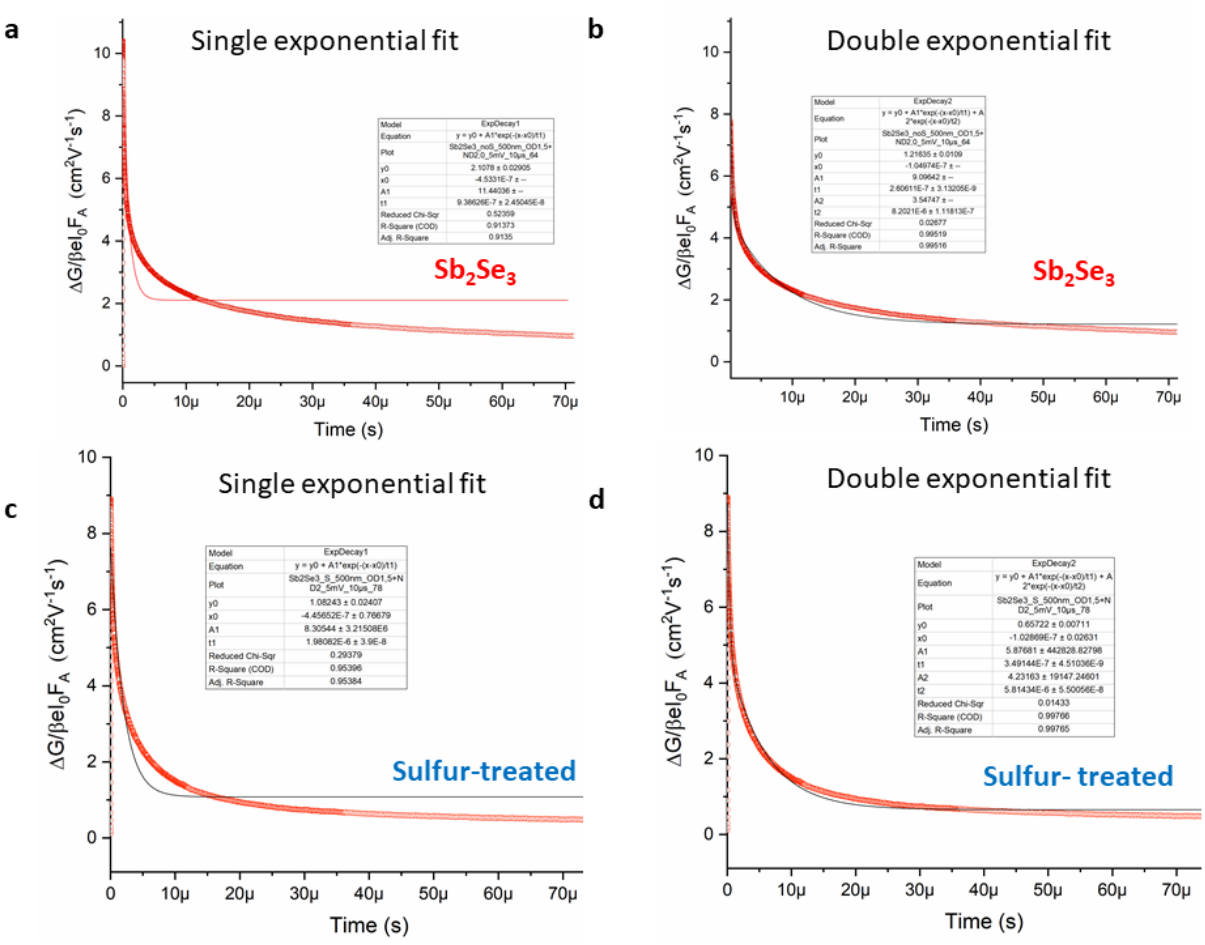

Figure S5. Single exponential fits of photoconductance vs time plots for **a** Sb_2Se_3 and **c** sulfur-treated film for 500 nm illumination. Double exponential fits of photoconductance vs time plots for **b** Sb_2Se_3 and **d** sulfur- treated for 500 nm illumination.

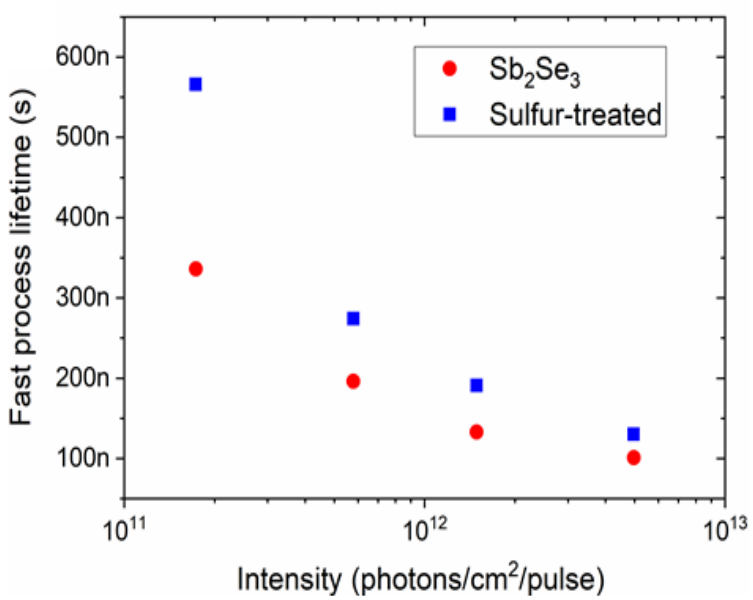

Figure S6. Determined lifetime for the fast process from a single exponential fit.

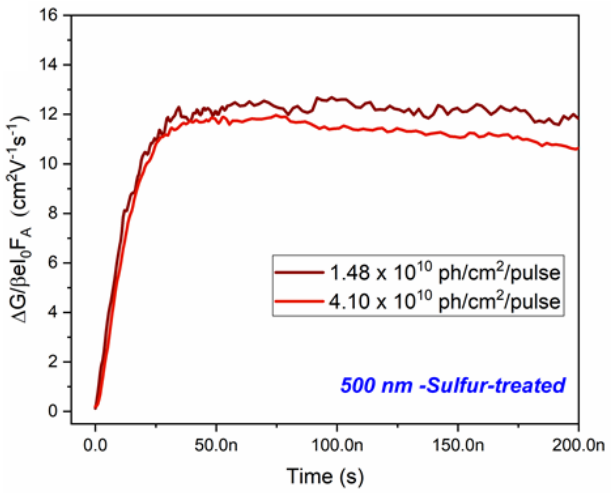

Figure S7. Photoconductance decay for sulfur-treated films under 500 nm illumination in the time scale of 200 ns showing the steady photoconductance signal under low light intensities.

Wavelength (nm)	Sb_2Se_3 (µs)	Sulfur-treated (µs)
500	0.34	0.56
650	0.268	0.352
800	0.265	0.357
950	0.210	0.339

Table S1. Fast process decay time constants for different excitation wavelengths for Sb_2Se_3 and sulfur-treated thin films (illumination intensities in the order of 10^{11} photons/cm^2/pulse)

Light intensities (photons/cm^2/pulse)	Sb_2Se_3 (µs)	Sulfur-treated (µs)
1.48×10^{10}	53.6	32.3
4.10×10^{10}	53.01	31.5
1.73×10^{11}	48.49	34.1
5.79×10^{11}	45.67	36.2
1.49×10^{12}	43.53	37.4
4.97×10^{12}	40.17	37.2

Table S2. Slow process decay time constants for different light intensities for Sb_2Se_3 and sulfur-treated thin films

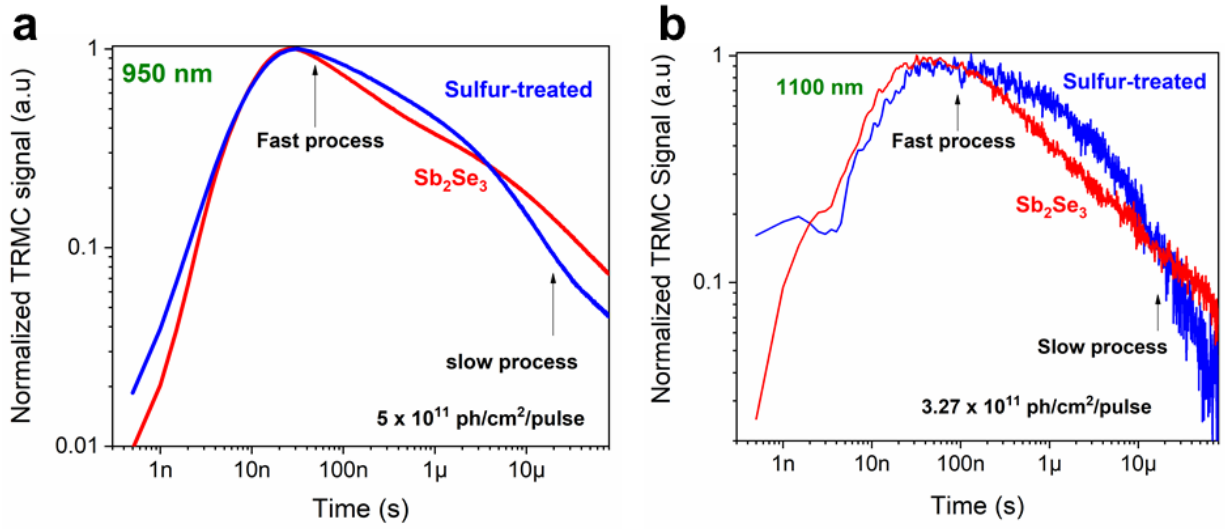

Figure S8. Normalized double log plots of Sb_2Se_3 and sulfur-treated films under **a** 950 nm **b** 1100 nm showing the fast process and slow process decay of the TRMC signal.

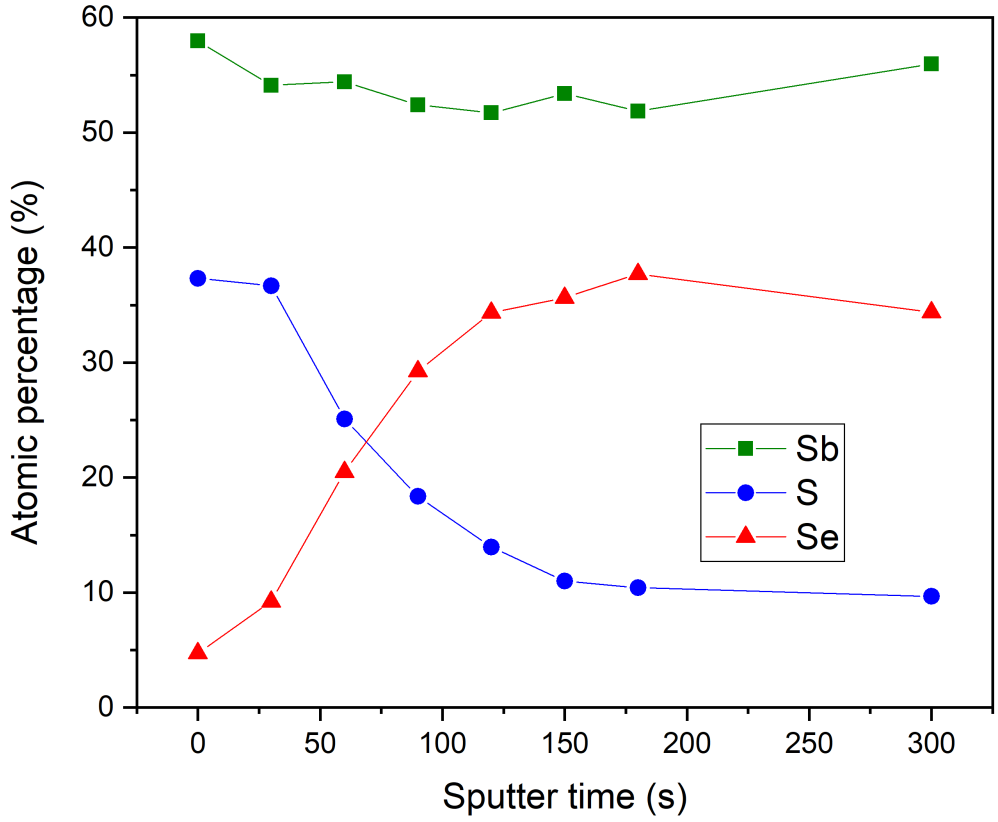

Figure S9. XPS sputter depth profile of sulfur-treated Sb_2Se_3 (300 s corresponds to a depth of 40 nm). Measurements were taken after each sputter step. Sb, S as well as Se concentrations are given according to X/(Sb + S + Se), disregarding contributions of adsorbates (O and C) at the surface.

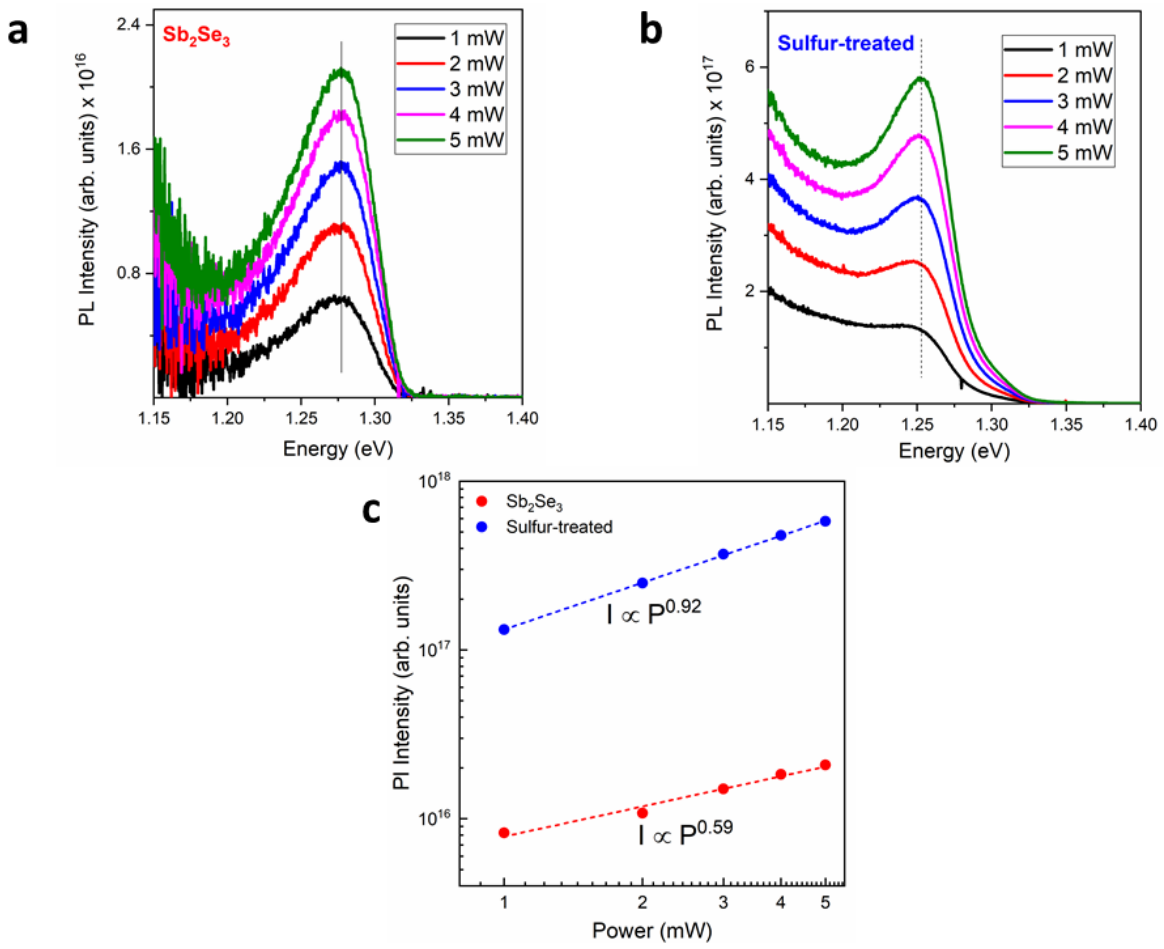

Figure S10. Power dependent PL spectra of **a** Sb_2Se_3 and **b** sulfur-treated films. **c** Power law fitting of PL intensity vs incident power for Sb_2Se_3 and sulfur-treated films.

This Work		Literature		
Sb_2Se_3	*Sulfur-treated*	*Sb_2Se_3 DFT*	*Sb_2Se_3 Experimental*	*Sulfur-treated*
45.13	27.69	43,46	80	15
60.03	42.65	49,55	84	22
72.44	59.051	56,58	105	28
84.81	82.83	68	117	33
120.31	95.18	69,72	120	41,42
177.08	106.53	84	122.6	44
191.2	118.83	88	131	51,52
205.28	141.41	94	151	63
213.52	153.65	107,111	155.2	68
222.71	189.74	117	181	82
256.03	254.07	122	189	88
375.02		124,126	189.6	150
		131	193	153
		132,142,143	210	220
		155	213	248
		156	225	216
		178	233	467
		180	234	473
		185	254	440
		187	373	
		190		
		205		
		211		
		213		

Table S3: Comparison of AVMs observed in Sb_2Se_3 reference samples, sulfur-treated Sb_2Se_3 samples with theoretical modes reported for Sb_2Se_3 and experimentally observed modes reported for Sb_2Se_3 and sulfur. The LFR peaks observed at 27.69 cm^{-1}, 42.65 cm^{-1} and 153.65 cm^{-1} match those of elemental sulfur. While the peak at 27.69 cm^{-1} can be attributed to the external surface vibrations of α-S_8 and the peak at 42.65 cm^{-1} can be attributed to similar surface modes of γ-S_8, the peak at 153.65 cm^{-1} is attributed to internal bond vibration of S_8 as consistent with reports in the literature that all the allotropes of S_8 have similar spectral feature at 153cm^{-1}.[4]

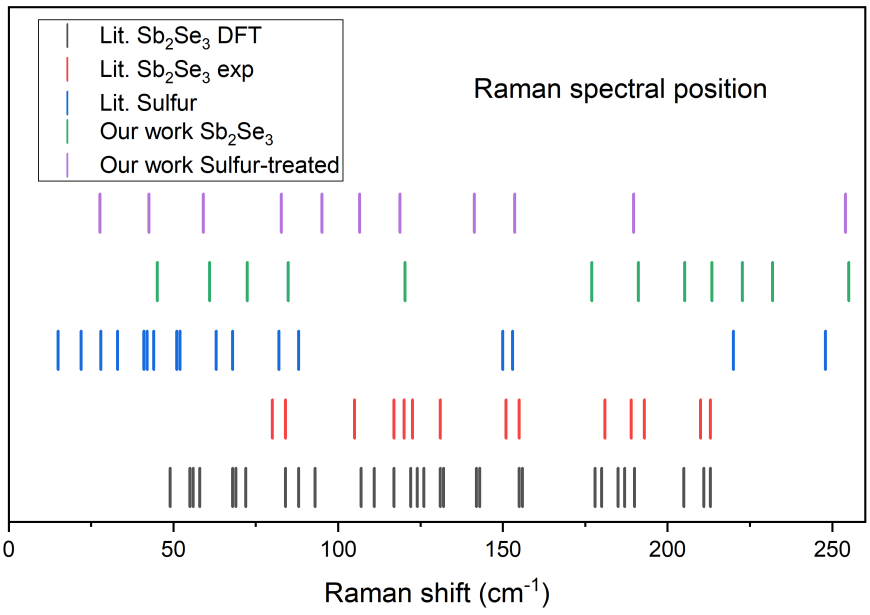

Figure S11. Graphical representation of LFR data presented in Table S1.

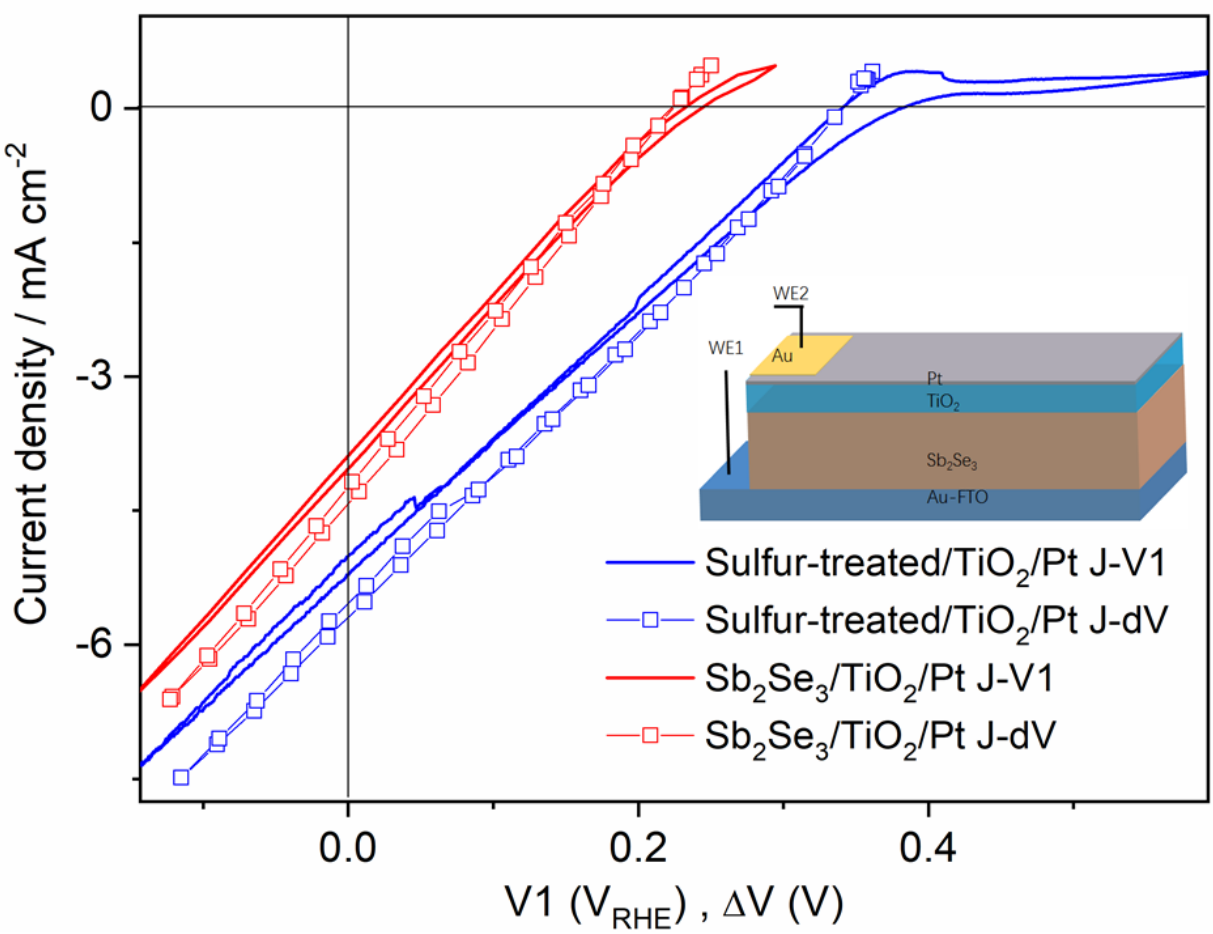

Figure S12. J-V1 and J-ΔV curves of $Sb_2Se_3/TiO_2/Pt$ and sulfur-treated/TiO_2/Pt showing the improvement of onset potential and the photovoltage upon sulfurization treatment. Schematic illustrating the device architecture of $Sb_2Se_3/TiO_2/Pt$ DWE under 1 sun illumination in 1 M H_2SO_4 (pH 0).

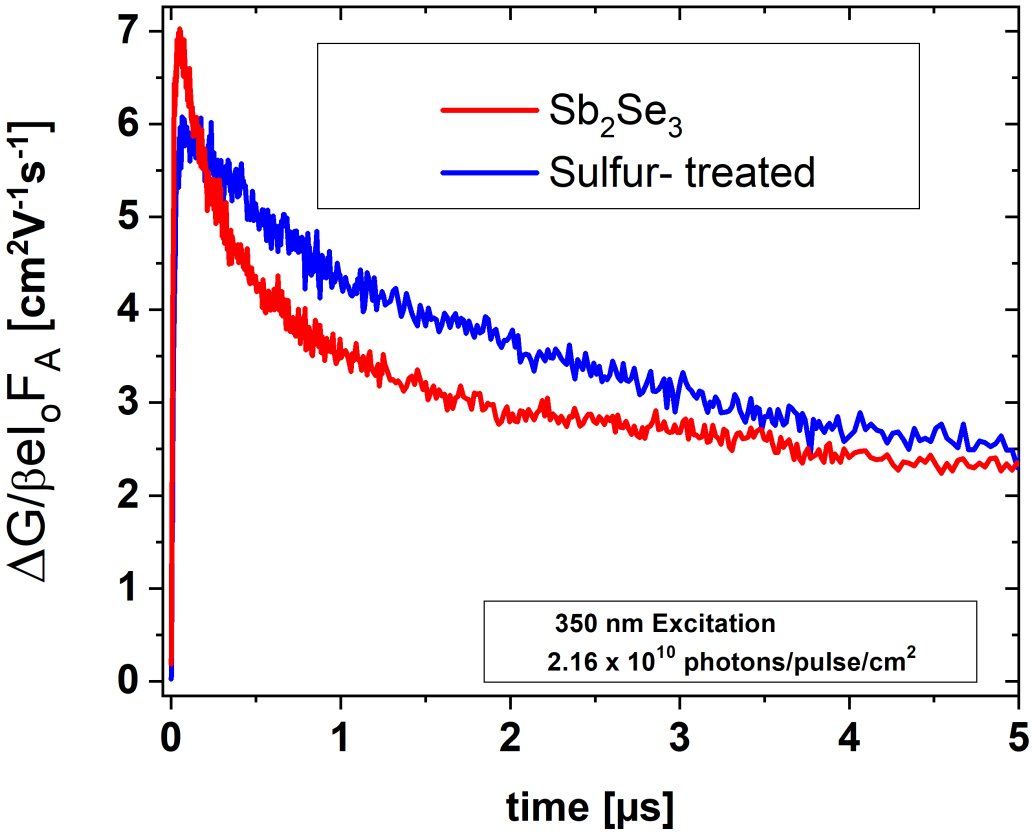

Figure S13. Transient photoconductance as a function of time induced by 350 nm laser light for 2.16 x 10^{10} photons/cm^2/pulse for Sb_2Se_3 and sulfur-treated films.

REFERENCES

[1] R. R. Prabhakar, W. Septina, S. Siol, T. Moehl, R. Wick-Joliat, S. D. Tilley, *J. Mater. Chem. A* **2017**, *5*, 23139.

[2] T. J. Savenije, A. J. Ferguson, N. Kopidakis, G. Rumbles, *J. Phys. Chem. C* **2013**, *117*, 24085.

[3] J. E. Kroeze, T. J. Savenije, J. M. Warman, *J. Am. Chem. Soc.* **2004**, *126*, 7608.

[4] C. Nims, B. Cron, M. Wetherington, J. Macalady, J. Cosmidis, *Sci. Rep.* **2019**, *9*.